REFERENCES AND NOTES

1. K. S. Ivanov, V. N. Puchkov, S. N. Ivanov, *Formation of the Earth's Crust of the Urals* (Nauka, Moscow, 1986); V. N. Puchkov, *Geotectonics* **27**, 184 (1993).
2. H. Echtler *et al.*, *Sci. Tech. Rep. STR95/01* (GeoForschungsZentrum, Potsdam, Germany, 1995).
3. The geological strip map is based on geologic field work and compilation of existing maps and data sets at a scale of 1:100,000 in cooperation with K. Ivanov and colleagues (Institute of Geology and Geochemistry, Russian Academy of Sciences, Ekaterinburg).
4. The energy source used for the experiment consisted of a five-truck vibrator group (each with a peak force of 10 tons) in the center of an 18-km geophone spread with a 50-m group spacing. Vibrator recording points were spaced 100 to 150 m apart, using a 30-s sweep (10 to 64 Hz), a 10-fold vertical stacking rate, and a 25-s recording time with a sampling rate of 4 ms, resulting in a nominal common depth-point fold of 60 to 90. This section represents processing of the eastern 420 km (out of 465 km) to 18-s TWT (two-way travel time) (~60 km depth). Processing steps (prestack): trace-individual static time corrections (topography and weathering layer effects), dynamic time corrections (source-receiver distance and subsurface velocity), amplitude corrections (surface condition, spherical divergence, and absorption), and noise wave elimination (refracted and shear wave energy). Final seismic displays were converted at 400 m above sea level. Depth-conversion of the time section after migration with a spatially variant time-velocity field was derived from the applied migration velocity functions. The uncertainty in the depth calculations caused by velocity inaccuracies is estimated to be ~3 to 5 km at a depth of 50 km. The high resolution of the seismic sections (>18,500 traces, 25-m spacing, 6400 samples per trace) was simplified for display purposes by building the envelope of each trace and summing each four adjacent traces.
5. A. M. C. Sengör, B. A. Natalyn, V. S. Burtman, *Nature* **364**, 299 (1993).
6. The Rb-Sr whole rock age of the Chebik granite is 267 ± 16 million years [K. S. Ivanov, S. N. Ivanov, Y. L. Ronkin, *Yearb. Ekaterinburg* **1994**, 171 (1995)].
7. M. A. Kamaletdinov, *The Nappe Structures of the Urals* (Nauka, Moscow, 1974).
8. D. Brown, V. N. Puchkov, J. Alvarez-Marron, A. Pérez-Estaún, *Earth Sci. Rev.* **40**, 125 (1996).
9. The Uraltau anticline comprises subduction-related high-pressure assemblages (eclogites and blueschists) [V. I. Lennykh, in *Pre-Ordovician History of the Urals*, S. N. Juanova, Ed. (Uralian Scientific Centre, Sverdlovsk, Russia, 1980), pp. 3–40]. The Kraka klippe (Fig. 1A) comprises westward-obducted ultramafic, oceanic assemblages rooted in the MUF [G. N. Savelieva, *Gabbro-Ultramafic Complexes of Ophiolites of the Urals and their Analogues in the Modern Oceanic Crust* (Nauka, Moscow, 1987); (7)].
10. J. H. Knapp *et al.*, *Science* **274**, 226 (1996).
11. J. H. Knapp *et al.*, *EOS* **76,** 549 (1995)
12. Special volume, *Tectonophysics* **238** (1994), and numerous references within.
13. R. Berzin *et al.*, *Science* **274**, 220 (1996).
14. Data acquisition in the southern Urals from June to November 1995 involved more than 100 scientists and technicians, not all of whom are named here, but whose contributions are gratefully acknowledged. The German part of URSEIS was funded through the program DEKORP 2000 (grant 03GT94101) by the German Federal Ministry of Science and Technology and was supported by the GeoForschungsZentrum Potsdam; the project also benefited from funding by the German Science Foundation, ROSCOMNEDRA (Committee on Geology and Use of Mineral Resources of the Russian Federation), the Continental Dynamics Program (NSF grant EAR-9418251 to Cornell University), Comisión Interministerial de Ciencia y Tecnología, Spain (grant AMB 95-0987E), and International Association for the Cooperation with Scientists from the Former Soviet Union grant 94-1857. This project forms part of EUROPROBE, whose members of the Urals Project have contributed significantly to this work.

29 May 1996; accepted 28 August 1996

Lithosphere-Scale Seismic Image of the Southern Urals from Explosion-Source Reflection Profiling

J. H. Knapp, D. N. Steer, L. D. Brown, R. Berzin, A. Suleimanov, M. Stiller, E. Lüschen, D. L. Brown, R. Bulgakov, S. N. Kashubin, A. V. Rybalka

Explosive-source deep seismic reflection data from the southern Ural Mountains of central Russia provided a lithosphere-scale image of the central Eurasian plate that reveals deep reflections (35 to 45 seconds in travel time; ~130 to 170 kilometers deep) from the mantle. The data display laterally variable reflectivity at the base of the crust that deepens beneath the central part of the profile, documenting a crustal thickness of ~55 to 60 kilometers beneath the axis of the orogen. These data provide an image of the structure of the crust and underlying mantle lithosphere in a preserved collisional orogen, perhaps to the base of the lithosphere.

Explosive-source deep seismic reflection profiling was conducted to (i) provide a high-resolution reflection image of the Mohorovičić discontinuity (the base of the crust, known as the Moho) across the entire orogen, (ii) document the lower crustal signature of the presumably unextended Uralian crust, and (iii) search for mantle structures (such as remnants of Paleozoic subduction) beneath the orogen. Experimental design was integrated with a coincident vibroseis survey (*1*).

The 465-km profile displays a reflective crust with a laterally variable reflection signature from the Moho (Fig. 1). On the western and eastern portions of the profile, the Moho is imaged at ~13 s (*2*), deepening toward the orogenic axis, where it is interpreted at the base of a general downward decrease in reflectivity at ~18 to 20 s (Fig. 1). Corresponding crustal thicknesses range from ~42 km beneath the East European platform and the western edge of the West Siberian basin to a projected maximum of 60 km in the central part of the profile. These data provide a near-vertical reflection image of a thickened Uralian crust, confirming earlier observations based on Russian deep seismic sounding data (*3*) and consistent with coincident wide-angle data collected by URSEIS '95 (*4*).

The Moho beneath the Trans-Uralian zone on the eastern end of the profile is imaged as a set of subhorizontal reflections beneath a region of west-dipping reflections and above a much less reflective upper mantle. Beginning at the position of the Troitsk fault, the Moho deepens abruptly into the central part of the profile, where the reflection Moho does not appear as a distinctive feature (Fig. 1). Amplitude decay analysis suggests that this change in Moho character is not an artifact of poor energy penetration; the seismic signal remains above ambient noise down to 25 to 30 s. Projection of the Moho beneath the diffuse lower crustal reflectivity is consistent with refraction results (*4*) and yields a maximum crustal thickness of 60 km. In the west, beneath the East European platform, the Moho is defined by a sharp, subhorizontal, continuous reflection at the base of a reflective lower crust. Further east, at the transition from the Pre-Uralian foredeep to the West Uralian zone, the Moho is offset downward by about 4 km and continues as a broadly arched, concave-downward, 1- to 3-s-thick band of reflections. This arched Moho forms the western flank of the Uralian crustal root and disappears into the diffusely reflective orogenic axis beneath the Central Uralian zone.

Mantle reflection fabrics, imaged primarily beneath the Uralian hinterland, can be categorized into three principal features: (i) gently west-dipping reflections at 35 to 45 s (a depth of ~130 to 170 km) [the Nikolaevka reflection sequence (NRS)], (ii) a subhorizontal band of reflections from 22 to 24 s (~85 km deep) [the Alexandrovka reflection sequence (ARS)], and (iii) a diffuse, east-dipping fabric that characterizes much of the upper mantle in the east (Fig. 2). The ARS consists of a thin (<0.25 s), complex band of subhorizontal reflections at ~24 s, continuous for at least 50 km across strike (Fig. 2). Although the

J. H. Knapp, D. N. Steer, L. D. Brown, Institute for the Study of the Continents, Cornell University, Ithaca, NY 14853, USA.
R. Berzin and A. Suleimanov, Spetsgeofisika, Moscow, 107140 Russia.
M. Stiller and E. Lüschen, GeoForschungsZentrum, D-14473 Potsdam, Germany.
D. L. Brown, Instituto de Ciencias de la Tierra, Consejo Superior de Investigaciones Cientificas–Barcelona, 08028 Spain.
R. Bulgakov, Bashneftegeofizika, Ufa, 450000 Russia.
S. N. Kashubin and A. V. Rybalka, Bazhenov Geophysical Expedition, Scheelite, 624051 Russia.

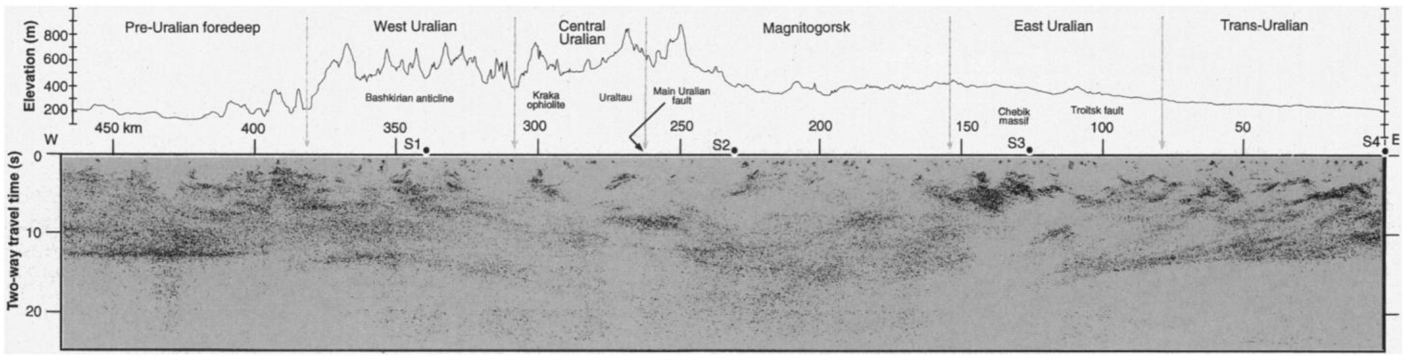

Fig. 1. Time-migrated section of explosive-source CMP data, shown to a depth of 25 s, with topography (exaggerated 50:1) and tectonic zones shown above.

travel time of the ARS matches that expected for a shear wave reflected from the Moho, the reflection appears to have a velocity more appropriate for a *P* wave. Additionally, comparison with the overlying west-dipping Moho suggests that this event is not a simple *P*-wave multiple. The ARS may represent a mantle shear zone developed during assemblage of the oceanic and microcontinental terranes in the Uralian hinterland. Diffuse reflection fabrics are observed in the upper mantle on the eastern and western parts of the profile and, upon migration, remain at upper mantle depths. Beneath the Trans-Uralian zone, east-dipping reflections from 20 to 40 s may be related to remnant fabrics of Paleozoic subduction (Fig. 2).

In the eastern part of the profile, the NRS consists of a series of reflections between 35 and 45 s that can be traced for more than 75 km (Fig. 2). These reflections include four west-dipping–to–subhorizontal reflection packages of ambiguous polarity and a signal-to-noise ratio of 2:1. The east-west extent of these reflections, crossing the dominant north-south structural strike of the orogen, implies that they do not originate as reflections from shallow crustal features located out of the plane. Discontinuous, subhorizontal events consisting of two bands of reflectivity occur at 55 s (~200 km) in the western part of the profile and are tentatively correlated with the NRS.

There are several possible interpretations for the origin of the NRS, including the base of the thermal lithosphere, a low-velocity shear zone, a fine-scale compositional variation, a relict west-dipping subduction zone, and fluids trapped within the mantle. Low-velocity zones have been identified at similar depths within central Eurasia in peaceful nuclear explosion data (*5*), and the NRS may correlate with these, implying a regional (>2000 km long) extent for this mantle signature. Because the polarity of the NRS reflections has not yet been determined with our existing *P*-wave reflection data, it is not possible to verify whether these reflections represent low or high velocities with respect to the surrounding mantle. However, the depth of the NRS is consistent with independent estimates for lithospheric thickness throughout Europe (*6*), and the geometry of the interpreted lithospheric boundary, shallowing from beneath the Archean crust of the East European craton to the accreted Paleozoic crust of central Eurasia, suggests a plausible correlation of lithospheric thickness with the age of crustal formation. Reflectivity at the base of the lithosphere has not been widely reported; however, a few near-vertical incidence reflection studies have recorded to these depths, and the higher frequencies used in reflection seismology should provide greater resolution of the lithosphere-asthenosphere boundary, particularly for small-scale structure within a velocity gradient. Regardless of whether the strain is localized at a basal boundary or distributed within a thick zone of the upper mantle, the Eurasian plate has been translated by hundreds of kilometers relative to the underlying asthenospheric mantle since the Late Paleozoic (*7*), a process that has ostensibly imparted strain fabrics and accordingly impedance contrasts in the lower mantle lid.

Previously identified seismic reflections from the mantle (*8*) occur between 20 and 30 s. In most cases, these are moderately to steeply dipping and migrate to considerably shallower levels (<80 km) in the mantle, making the NRS the deepest reflection imaged with the common midpoint (CMP) technique. It remains unclear whether the fabrics and reflections observed in the Uralian mantle are preserved from Paleozoic orogeny or represent a younger history of structural and thermal evolution of the mantle lithosphere. If these mantle reflections represent structures created during and preserved since the collision, the URSEIS '95 data provide evidence that stabilization of continental lithosphere took place directly after orogeny, and relatively little modification of the mantle has taken place since. Alternatively, younger development of these features in the mantle, either as structural fabrics or as compositional differentiation, would imply that such mantle processes can take place without noticeably affecting the overlying crustal column.

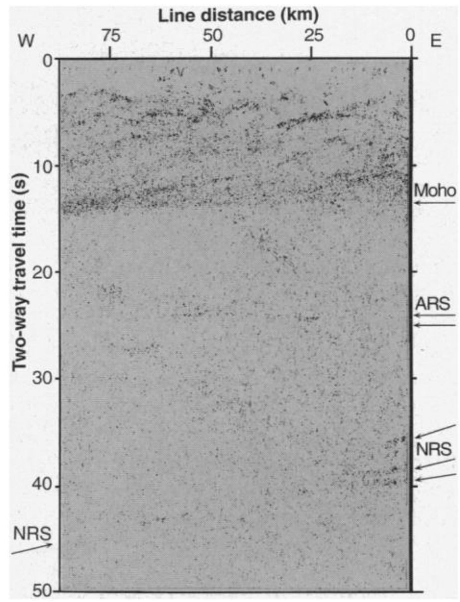

Fig. 2. Unmigrated section of the eastern end of the explosive-source CMP data, illustrating the position, geometry, and reflective character of the NRS, the ARS, diffuse east-dipping mantle fabrics, and the Moho.

REFERENCES AND NOTES

1. R. Berzin *et al.*, *Science* **274**, 220 (1996); H. P. Echtler *et al.*, *ibid.*, p. 224. The experimental design consisted of a recording spread with 360 channels at a 50-m station spacing over 18 km, recorded by an I/O System 2 (Houston, TX). Eighty-kilogram shots were repeated twice (forward and backward shooting) every 3 km in two 30-m-deep shot holes in an off-end configuration; the signals were recorded for 65 s at a 4-ms sample rate. Processing before stack: trace editing, static time corrections to correct for elevation changes, time and space variant filtering, amplitude corrections (spherical divergence and absorption), lateral trace equalization, frequency-time deconvolution, time-phase velocity filtering, and application of a time and space variant velocity field. Processing after stack: frequency-time deconvolution filter, coherency filter, migration [using smoothed interval velocity function derived from the velocity model of Carbonell *et al.* (*4*)]. Final display, 1:1 at 6 km/s.
2. All travel times are given in two-way travel time. Cor-

responding depths are derived from an average crustal velocity of 6 km/s and mantle velocity of 8 km/s.
3. A. V. Egorkin and A. V. Mikhaltsev, in *Superdeep Continental Drilling and Deep Geophysical Sounding*, K. Fuchs *et al.*, Eds. (Springer-Verlag, Heidelberg, Germany, 1990), pp. 111–119.
4. R. Carbonell *et al.*, *Science* **274**, 222 (1996).
5. J. Mechie *et al.*, *Phys. Earth Planet. Inter.* **79**, 269 (1993); K. Priestley, J. Cipar, A. Egorkin, N. Pavlenkova, *Geophys. J. Int.* **118**, 369 (1994); T. Ryberg, K. Fuchs, A. V. Egorkin, L. Solodilov, *J. Geophys. Res.* **100**, 18151 (1995).
6. G. F. Panza, *Second European GeoTraverse Workshop* (European Science Foundation, Strasbourg, France, 1985), pp. 47–55.
7. W. McKerrow and C. Scotese, *Paleozoic Paleogeography and Biogeography* (Geological Society of London, London, 1990).
8. J. E. Lie, T. Pedersen, E. S. Husebye, *Nature* **346**, 165 (1990); D. J. Baird, J. H. Knapp, D. N. Steer, L. D. Brown, K. D. Nelson, *Geology* **23**, 431 (1995); S. E. McGeary and M. R. Warner, *Nature* **317**, 795 (1985); M. Warner *et al.*, *Geology* **24**, 39 (1996).
9. Funding for this research was provided by the Continental Dynamics Program (NSF grant EAR-9418251 to Cornell University), ROSCOMNEDRA (Committee on Geology and Use of Mineral Resources of the Russian Federation), the program DEKORP 2000 (grant 03GT94101) by the German Federal Ministry of Science and Technology, and the GeoForschungsZentrum Potsdam; the project also benefited from funding by the German Science Foundation, Comisión Interministerial de Ciencia y Tecnología (Spain) (AMB 95-0987E), and International Association for the Cooperation with Scientists from the Former Soviet Union grant NTAS 94-1857. This research was developed and carried out in association with the EUROPROBE Urals Project. This is Institute for the Study of the Continents contribution 228.

29 May 1996; accepted 28 August 1996

A Mini-Surge on the Ryder Glacier, Greenland, Observed by Satellite Radar Interferometry

Ian Joughin, Slawek Tulaczyk, Mark Fahnestock, Ron Kwok

Satellite radar interferometry reveals that the speed of the Ryder Glacier increased roughly threefold and then returned to normal (100 to 500 meters/year) over a 7-week period near the end of the 1995 melt season. The accelerated flow represents a substantial, though short-lived, change in ice discharge. During the period of rapid motion, meltwater-filled supraglacial lakes may have drained, which could have increased basal water pressure and caused the mini-surge. There are too few velocity measurements on other large outlet glaciers to determine whether this type of event is a widespread phenomenon in Greenland, but because most other outlet glaciers are at lower latitudes, they should experience more extensive melting, making them more susceptible to meltwater-induced surges.

Discharge of ice through outlet glaciers represents a substantial part of the mass loss of the Greenland and Antarctic ice sheets and thus has a major impact on their mass balances. Few in situ observations have been made with which to assess the variability of outlet glacier flow (*1*). Satellite radar interferometry now provides an important means for measuring ice velocity (*2–4*). Using this technique, we documented a radical pulse in the speed of the Ryder Glacier, an outlet glacier at the northern edge of the Greenland Ice Sheet. This pulse or "mini-surge" (*5*) represents a significant, although short-term, increase in discharge from the ice sheet. There are only a few outlet glaciers from the large ice sheets on which substantial speed variations have been observed (*6*), and none have exhibited a similar short pulse of enhanced motion. Short pulses in speed have been documented on several valley glaciers, such as a large tidewater glacier in Alaska (*7*), and the Variegated Glacier during an extended surge (*8*).

The Ryder Glacier (Fig. 1) drains a basin of 28,300 km^2, about 1.7% of the inland ice area. The total accumulation for the basin is a water equivalent of 5.0 km^3/year (*9*), making the Ryder a moderately sized outlet glacier for Greenland. The Ryder has two branches, which converge at an elevation of 1000 m; it then flows out through the Sherard Osborn Fjord. At the head of the fjord, a prominent ice ridge is oblique to the fjord axis (Fig. 1). This feature is likely generated by ice flow over a subglacial bedrock ridge and shifts flow to the western side as ice enters the fjord. Ice backed up behind the ridge forms an ice plain (slope of ~0.002) covered by several large lakes (Fig. 1).

We created several interferograms of the Ryder from images taken by the synthetic aperture radars on board the ERS-1 and ERS-2 satellites. There are striking differences between the interferograms for September and October of 1995 (Fig. 2) over the fast-moving portion of the glacier below about 1100 m. The density of fringes (color cycles) in the October interferogram (Fig. 2B) is much greater than that in the September interferogram (Fig. 2A), indicating that flow was more rapid in October. The magnitude of the difference is far greater than the few fringes that may be attributable to differential propagation delays from atmospheric effects (*10*), and the patterns of enhanced fringes are clearly related to ice flow. Farther down-glacier, on the fastest moving parts, the pattern of fringes is lost completely in the October interferogram, whereas prominent fringes are still visible over this part of the September interferogram. The fringe loss is the result of gradients in velocity beyond the rate that can be measured with a 1-day separation of images. In the region where there is a rapid increase in the flow speed (white boxes in Fig. 2, A and B), the pattern of fringes is more complex (Fig. 2C) than it had been before the speedup.

The across-track component of velocity for the September observation (Fig. 3A) agrees well with another velocity map made from ERS-1 images acquired in March 1992 and appears to represent velocity in the normal flow mode of 100 to 500 m/year for most of the glacier. A map of the difference

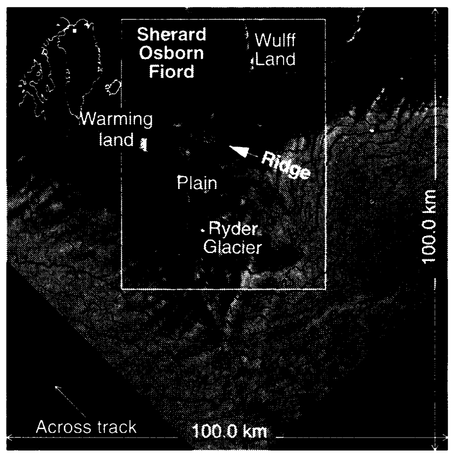

Fig. 1. ERS-1 amplitude image of Ryder Glacier acquired on 18 March 1992 at the location indicated by a solid-white box on the inset map. The pattern of low backscatter at the ice margin increasing to bright backscatter further inland is the result of the different scattering properties of the bare-ice, wet-snow, and percolation facies (*19*). The locations where lakes existed during the previous melt season appear as bright spots a few kilometers in diameter. Elevation contours at 50-m (thin) and 100-m (thick) intervals are plotted over ice-covered portions of the scene. We differenced pairs of interferograms to remove the displacement effect (*20*) to create this digital elevation model (DEM). The relative accuracy of the DEM is on the order of a few meters, although there may be long-wavelength errors of up to several tens of meters. White outlined box indicates area shown in Fig. 2.

I. Joughin and R. Kwok, Jet Propulsion Laboratory, California Institute of Technology, MS 300-235, 4800 Oak Grove Drive, Pasadena, CA 91109, USA.
S. Tulaczyk, Division of Geological and Planetary Sciences, California Institute of Technology, MS 170-25, Pasadena, CA 91125, USA.
M. Fahnestock, Joint Center for Earth System Science, Department of Meteorology, University of Maryland at College Park, College Park, MD 20742, USA.